# To Be or Not to Be a Molecular Ion: The Role of the Solvent in Photoionization of Arginine.
# Supplemental Information.

Alexandre Barrozo[a], Bo Xu[b], Anastasia O. Gunina[a], Michael I. Jacobs[b],

Kevin Wilson[b], Oleg Kostko[b], Musahid Ahmed[b], Anna I. Krylov[a]

[a]Department of Chemistry, University of Southern California, Los Angeles, California 90089-0482

[b]Chemical Sciences Division, Lawrence Berkeley National Laboratory, Berkeley, CA 94720

[c]The Hamburg Centre for Ultrafast Imaging, Luruper Chaussee 149, 22671 Hamburg, Germany

## I.   EXPERIMENTAL DETAILS

### A.   Materials

Initial 0.1 mol/L arginine (Sigma-Aldrich, ≥98%) solutions were prepared with highly demineralized water. pH values of 1, 4, 7, 9 and 13 (±0.1) were adjusted either with hydrochloric acid or sodium hydroxide.

### B.   VUV mass spectrometry

The apparatus used to measure mass spectra of fragile arginine incorporated an aerosol particle mass spectrometer coupled to a VUV synchrotron radiation source[1]. Arginine aqueous nanoparticles were generated by atomizing the corresponding aqueous solution using a high flux atomizer (Model 3076, TSI). $N_2$ was used as carrier gas. The size distribution of the nanoparticles was measured with a commercial scanning mobility particle sizer (SMPS, TSI). The distribution was broad, with a mean diameter of 170 nm. After passing through a set of aerodynamic lenses, the nanoparticles were tightly focused into a beam, which was then impacted on a copper heater located between the time-of-flight (TOF) optics of the VUV mass spectrometer. In this experiment, the temperature of the heater was 473 K. The gas-phase molecules produced by particle vaporization were ionized with tunable VUV light generated from Beamline 9.0.2 at the Advanced Light Source, Lawrence Berkeley National Laboratory. A home-made dual-stage pulsed acceleration TOF was used to transfer the ions

across a field free tube, where the ions were subsequently detected on a microchannel plate (MCP) detector. The resulting signal was passed through a preamplifier and collected with a multiscaler (FAST Comtec P7886). TOF mass spectra were collected in 0.1 eV steps from 7.5 to 10 eV. After correcting for photon flux and energy calibration, the photoionization efficiency curves were extracted for each mass.

## C.   VUV photoelectron spectroscopy

To obtain VUV photoelectron spectra of arginine aqueous nanoparticles, which were generated and focused as described above, we used a velocity map imaging (VMI) spectrometer[2]. At a mean diameter of 170 nm, the nanoparticle provides a nanoscaled bulk solution environment, allowing the electronic structures of arginine to be probed in the solution phase. The focused nanoparticles beam passed through two differential pumping regions and entered the interaction region of the VMI spectrometer. The VUV beam intersected the nanoparticles beam at 90°. The electron optics of the VMI spectrometer were biased to achieve "velocity map" conditions[3], in which all electrons with the same momentum in the plane of the detector were mapped onto the same point of the detector. The detector comprised a 75 mm diameter dual MCP coupled to a fast phosphor screen (both made by Photonis). The electron images were recorded with a complementary metal-oxide-semiconductor camera. Typical accumulation time for an image was 3 minutes and the images were collected in triplicate. A background image was collected with an inline particle filter inserted to remove all nanoparticles from the beam, and was subtracted from the data image. We obtained the velocity distributions from the background-subtracted images by performing an angular integration of the images as a function of radius using the BASEX algorithm[4]. The spectrometer was calibrated with $5p_{3/2}$ and $5p_{1/2}$ of Xe, in order to relate radial position in the image to electron kinetic energy. Electron binding energies reported here are with respect to vacuum.

## D.    Arginine fragments appearance energies

TABLE S1: Estimates of the appearance energies extracted from the photoionization efficiency curves for various fragments of arginine (see Fig. S1). Due to absence of a sharp onset in some of the curves, not all the appearance energies could be determined; these cases are marked with an asterisk.

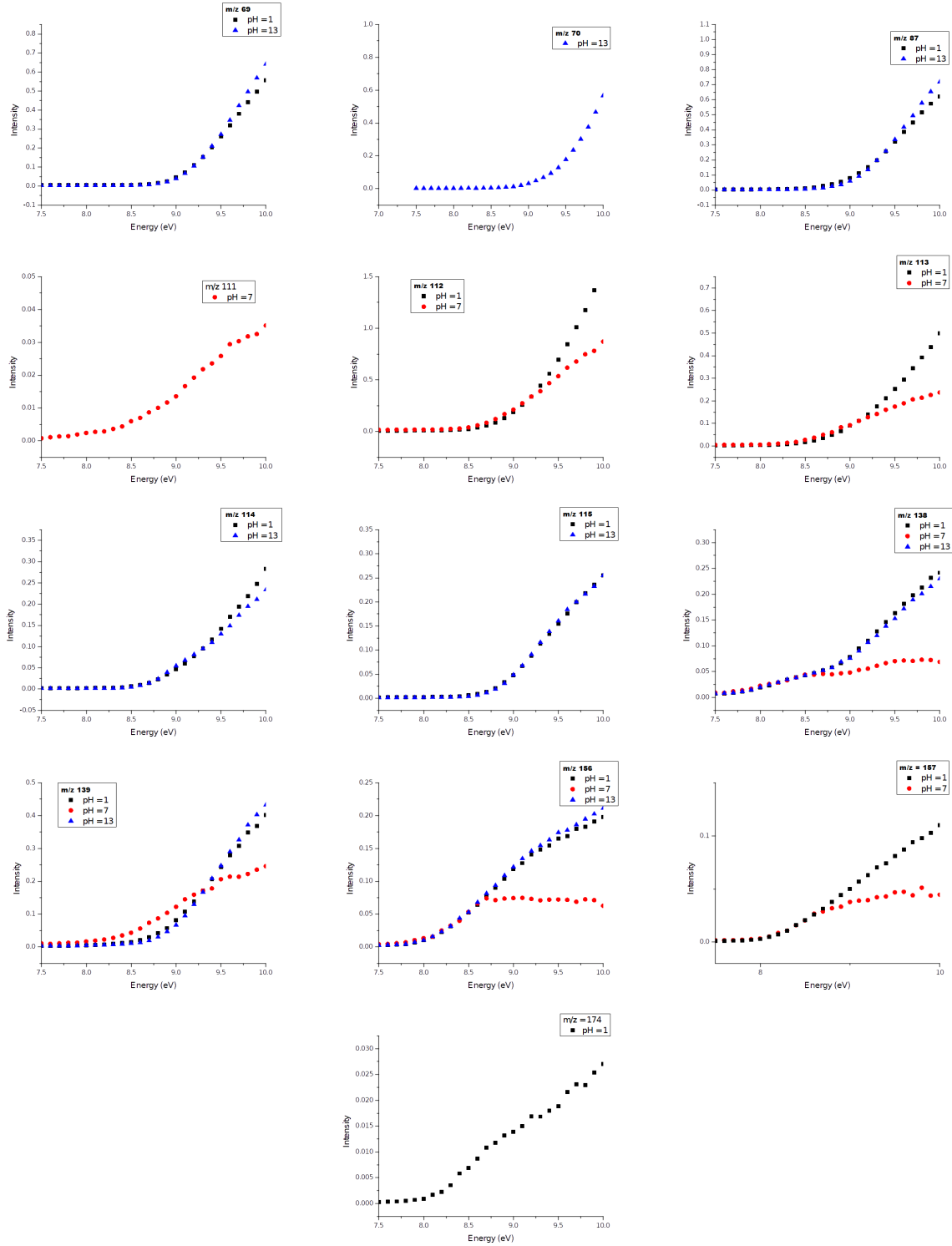| m/z | pH = 1 | pH = 7 | pH = 13 |
|-----|--------|--------|---------|
| 69  | 9.0    | –      | 9.1     |
| 70  | –      | –      | 9.2*    |
| 87  | 8.9    | –      | 9.0     |
| 111 | –      | 8.2    | –       |
| 112 | 8.9*   | 8.5    | –       |
| 113 | 8.8*   | 8.4    | –       |
| 114 | 8.8*   | –      | 8.7     |
| 115 | 8.7    | –      | 8.8     |
| 138 | 7.7    | 7.7    | 7.7     |
| 139 | 8.7    | 8.3    | 8.8     |
| 156 | 7.9    | 7.9    | 8.0     |
| 157 | 8.1    | 8.0    | –       |
| 174 | 8.0    | –      | –       |

FIG. S1: Photoionization efficiency curves of various fragments of arginine. Large differences can be seen between the data at pH 7 and the other data. There were problems with the aerosol beam clogging the orifice of the spectrometer for the pH 7 measurements through the scans. Although there are differences in the onsets for different fragments, they are consistent between the different pH values.

## E.   Water photoionization spectra

To investigate solvent effects in photoionization of arginine, we carried out photoionization measurements with arginine's aqueous nanoparticles. In these experiments, the spectra contain the contributions from bulk water ionization. To interpret these spectra, one needs to disentangle the spectral signatures of the solute (arginine) and the bulk solvent (water). The lowest IE of gas-phase water is 12.75 eV[5,6] whereas the onset of bulk water ionization is lower, at around 10 eV[6,7]. The experiment with photons of 15 eV shows prominent contributions of water ionization. Fig. S2 shows the spectra obtained with 12 eV and 15 eV photons, together with the bulk water spectrum from Winter *et. al.*[6] The water ionization spectrum was obtained by digitizing Fig. 3 from Ref. 6 using WebPlotDigitizer[8] and normalized to match the scale of our experimental spectra.

It is clear that beyond 10 eV the spectra contain contributions from bulk water ionization and that the spectra obtained with 15 eV photons are affected more than the spectra obtained with 12 eV photons. The first bulk water peak, which appears between 10 and 12.5 eV, matches the region of the second broad peak in our 15 eV spectra. Thus, we infer that the drop of intensity at 10 eV corresponds to the end of the arginine's peak and the beginning of the bulk water signal. Consequently, in our analysis we focus on the signal below 10 eV, which can be confidently attributed to the arginine species alone. As discussed below, the problem of disentangling solute and solvent contributions is compounded by possible contributions from the first solvated shell (in which water molecules are strongly affected by the interactions with charged groups of the solute) and counterions.
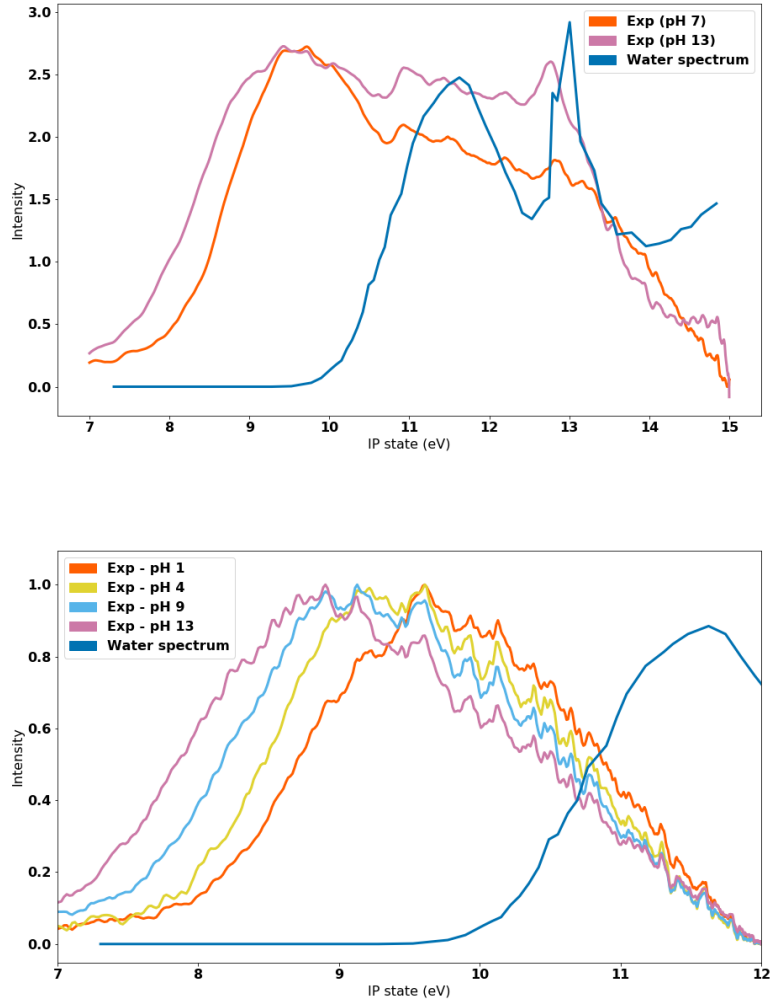
FIG. S2: Comparison between the experimental photoelectron spectra of aqueous arginine aerosols at various pH and water solution spectrum digitized from Fig. 3 in Ref. 6. Top: spectra measured at photon energy of 15 eV. Bottom: spectra measured at photon energy of 12 eV. The intensities are arbitrary.

## II.   THEORETICAL METHODS AND COMPUTATIONAL DETAILS

All calculations were carried out using *Q-CHEM* electronic structure package[9,10] and *GROMACS* software[11].
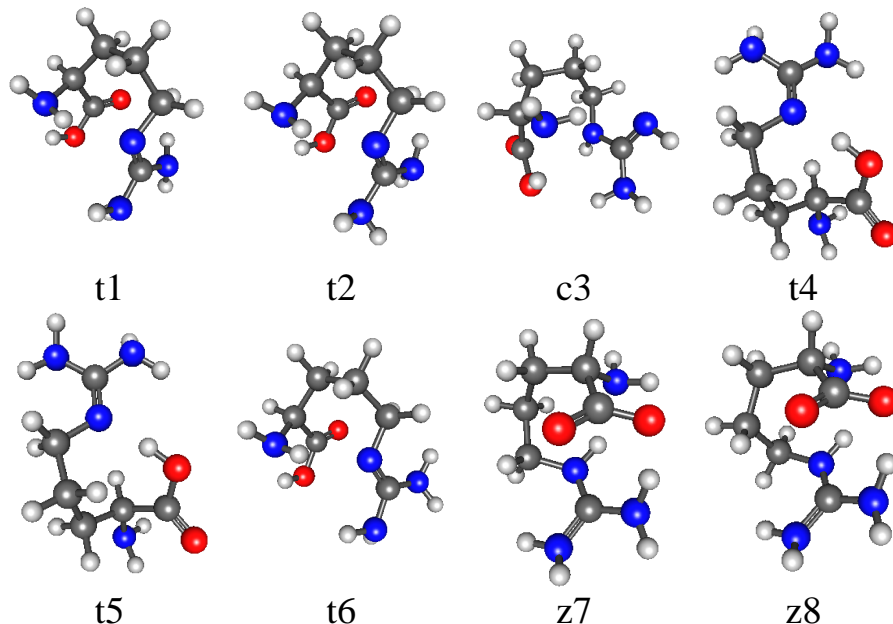
### A.   Gas phase simulations



FIG. S3: Isomers of arginine considered in this work. Tautomeric, canonical, and zwitterionic conformers are denoted by *t*x, *c*x, and *z*x, respectively. The numbering corresponds to the CCSD/6-31++G(d,p) total energies.

Equilibrium geometries of neutral arginine conformers (Fig. S3) were taken from Ref. 12, where they were computed at the MP2/6-31++G(d,p) level of theory. The structures were labeled according to the order of CCSD/6-31++G(d,p) total energies[12] (*e.g.*, *t*1 corresponds to the lowest-energy tautomeric form). We performed calculations of vertical ionization energies (VIEs) and Dyson orbitals of selected isomers using EOM-IP-CCSD/aug-cc-pVDZ at the above equilibrium geometries. To analyze the stability of ionized arginine in the gas phase, we optimized the structures of the cations using $\omega$B97X-D3/6-31++G(3df,2pd) starting from the geometries of the neutral isomers, which represent the Franck-Condon structures corresponding to vertical ionization. We computed AIEs as the differences between the EOM-IP-CCSD energies of the cations and the CCSD energies of the neutrals at

the respective equilibrium structures. The reported AIEs also include zero-point vibrational energy contributions computed with $\omega$B97X-D3/6-31++G(d,p) at the geometries optimized at the same level of theory. Dyson orbitals at the Franck-Condon and relaxed structures are shown in Fig. S4. VIEs and AIEs for non-dissociating isomers are collected in Fig. S5.
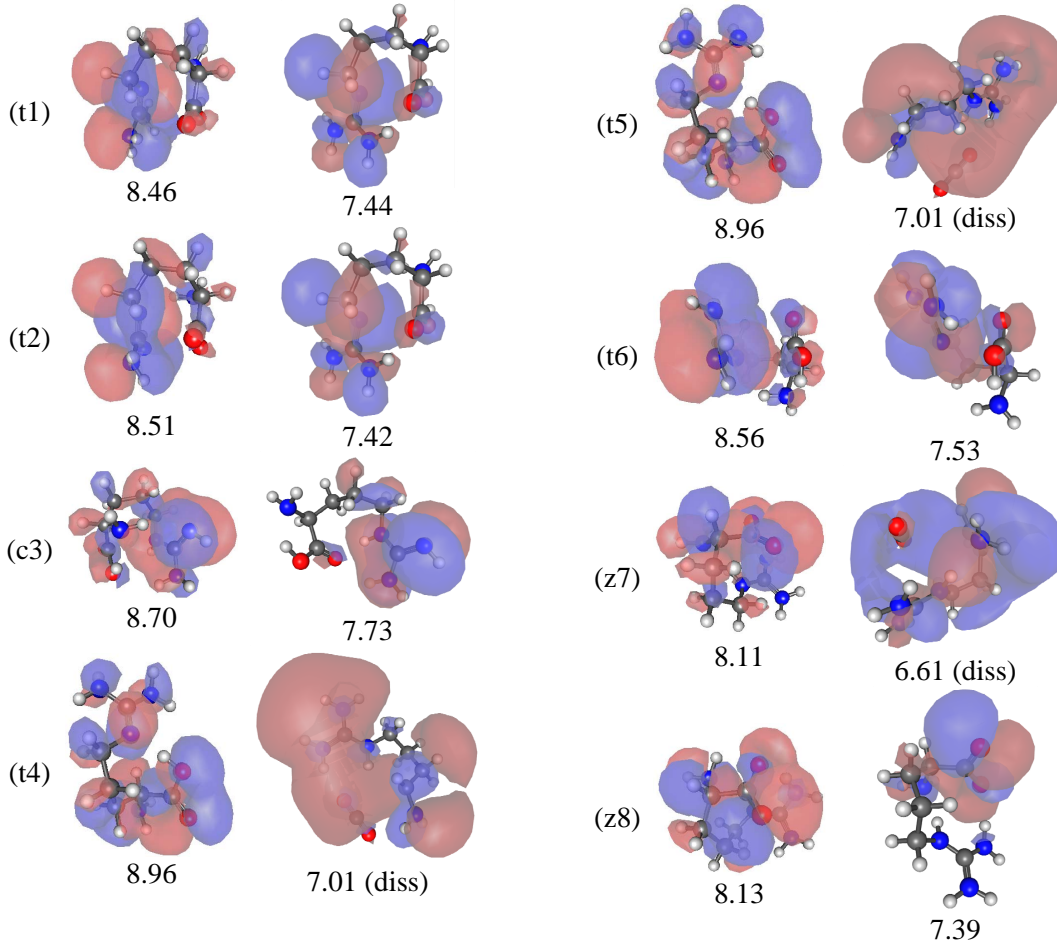


FIG. S4: VIEs/AIEs and Dyson orbitals of different isomers of arginine at the Franck-Condon (left columns) and relaxed (right columns) structures in the gas phase.

To model the impact of ionization, we carried out *ab initio* molecular dynamics (AIMD) simulations for cationic species with $\omega$B97X-D3/6-31++G(d,p). The trajectories were initiated from the neutral equilibrium geometry, with the initial velocities randomly sampled from the Maxwell-Boltzmann distribution at 10,000 K ($k_B T \sim 1$ eV of excess energy), 1,000 K ($\sim 0.1$ eV of excess energy), and 400 K. The 400 K temperature is the approximate temperature of the heater and 10,000 K is the temperature corresponding to a maximal expected excess energy from a photon (the difference between the lowest calculated VIE and the beam
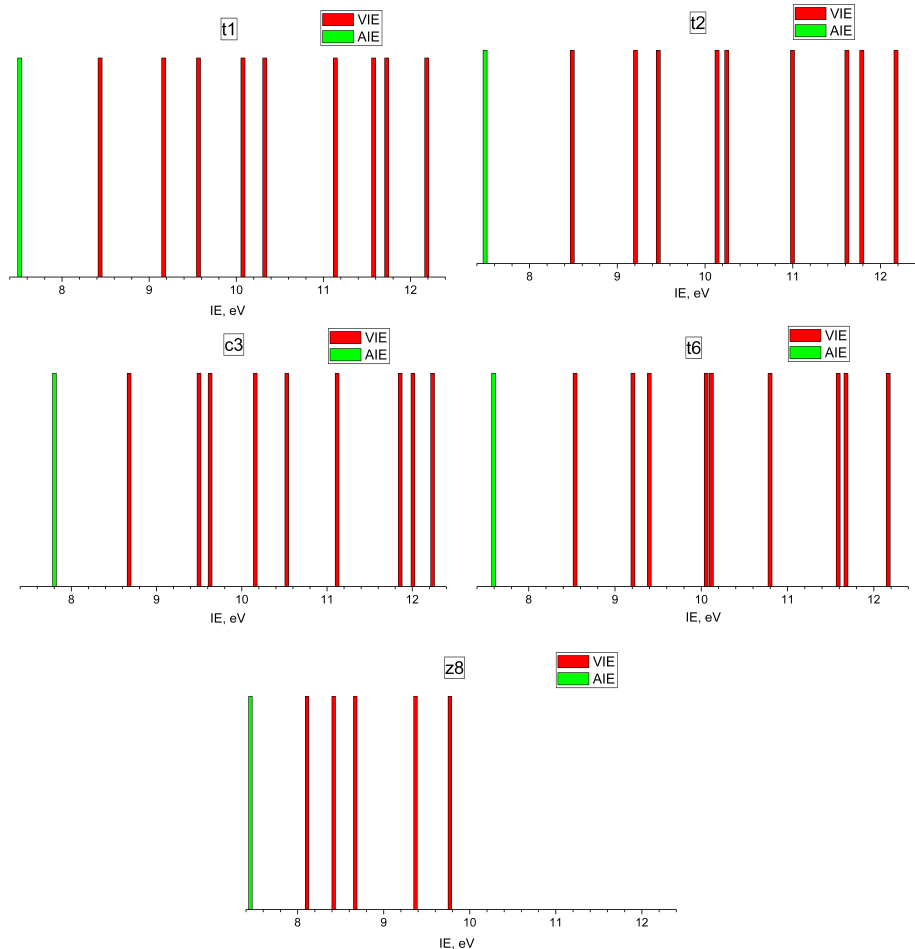
FIG. S5: Stick spectra showing the lowest nine VIEs (red) and the lowest AIE (green) for the $t1$, $t2$, $c3$, $t6$, and $z8$ isomers of gas-phase arginine.

energy). No thermostat was applied in these simulations, as appropriate for modeling the dynamics of isolated gas-phase molecules. The trajectories were propagated using 0.48378 fs (20 a.u.) time-step for 20,000 steps, resulting in 9,675 ps simulation time.

Using the same setup, we also carried out AIMD simulations of the neutral arginine with the initial velocities sampled from the Maxwell-Boltzmann distribution at 400 K. In these calculations, the energies and gradients were calculated using unrestricted Kohn-Sham DFT with an appropriate SCF guess.

## B. Condensed-phase simulations using implicit solvent

To model ionization in the condensed phase, we performed geometry optimizations of aqueous neutral and ionized arginine with $\omega$B97X-D3/6-31++G(d,p)/CPCM. Fig. S6 shows
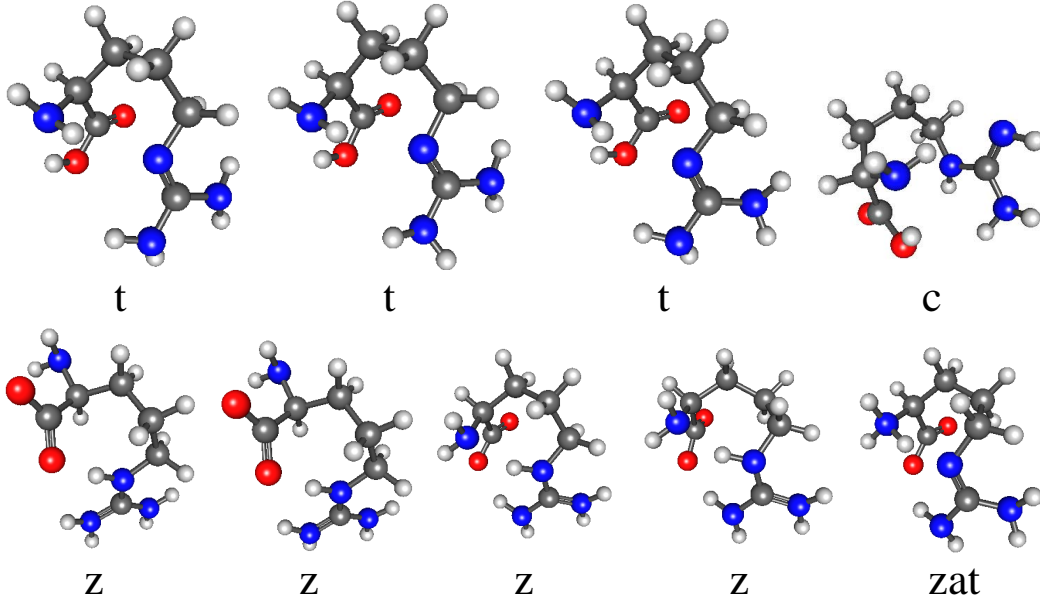
FIG. S6: Isomers of arginine (neutral forms) in water computed using $\omega$B97X-D3/6-31++G(d,p)/CPCM. $t$ denotes tautomeric type conformers, $c$ denotes canonical type, $z$ and $zat$ denote zwitterionic forms.

the resulting neutral structures. In addition to the structures similar to the ones from gas phase, we introduced a new zwitterionic structure, denoted $zat$.

Optimization of ionized species with CPCM did not result in dissociation. Most conformers converged to the structures of the same type as neutrals, except for $z8$ structure that converged to a new type denoted $zat$. Apart from $zat$, the optimized structures of the solvated cations resemble those of the corresponding non-dissociative gas phase cations.

## C. Condensed-phase simulations using explicit solvent

In the explicit-solvent calculations, we considered the following forms:

- Zwitterionic structure (labeled $z$ in Fig. 1 in the main text) without counterions (this is the dominant form at high pH);

- Carboxyl-to-amino zwitterionic structure (labeled $zac$ in Fig. 1 in the main text, similar to gas-phase zwitterion $zat$) without counterions;

- Singly protonated zwitterionic form (labeled $p$ in Fig. 1 in the main text) with a Cl$^-$ counterion (this is the dominant protonated form at neutral pH);

TABLE S2: Total energies (hartree) for various aqueous isomers of non-protonated and singly protonated arginine as well as the respective ionized species computed at the $\omega$B97X-D3/6-31++G(d,p)/CPCM level of theory (shown graphically in Fig. 3 in the main text).

| type (gas phase label) | initial | ionized |
|---|---|---|
| $t$ ($t1$) | -606.474 871 | -606.270 892 |
| $t$ ($t2$) | -606.474 778 | -606.270 904 |
| $c$ ($c3$) | -606.476 324 | -606.257 184 |
| $z$ ($t4$) | -606.494 370 | -606.291 747 |
| $z$ ($t5$) | -606.494 367 | -606.291 705 |
| $t$ ($t6$) | -606.475 146 | -606.270 903 |
| $z$ ($z7$) | -606.493 004 | -606.263 392 |
| $z$ ($z8$) | -606.494 870 | -606.280 637 ($zat$) |
| $zat$ | -606.485 862 | – |
| $p$ | -606.958 710 | – |
| $pg$ | -606.948 913 | – |

- Singly protonated at the guanidine group form (labeled $pg$ in Fig. 1 in the main text; this is the lowest energy protonated structure in the gas phase[12]) with a Cl$^-$ counterion.

For equilibrium sampling, we used molecular dynamics (MD) with the OPLS-AA force field[13] and TIP3P parameters to describe water. We have chosen OPLS-AA force field, which was designed to reproduce conformational energies and non-bonded parameters, including hydrogen bonding, because it was shown to work well for charged arginine isomers in the gas phase[14]. The partial charges were chosen based on the available OPLS-AA charges, as implemented in GROMACS. The arginine forms were solvated in a cubic box (45 Å long in each dimension) with periodic boundary conditions.

We prepared the initial structures by taking the corresponding gas-phase structures[12]. Initial velocities were randomly sampled from the Boltzmann distribution at 300 K. The trajectories were propagated using 2 fs time step, with a removal of the translation of center of mass every 100 steps, following the default settings in GROMACS. We started with an equilibration of 100 ps in the NVT ensemble using velocity rescaling at every 10 steps. Subsequently, we performed a 100 ps simulation for density equilibration in the NPT ensemble, using the same thermostat setup and including a Parrinello-Rahman barostat with pressure coupling at every 10 steps and $\tau_p$ of 2 ps. We then continued the simulation for another 1 ns to obtain snapshots for computing the photoionization spectra. The snapshots were taken every 10 ps from this 1 ns simulation, resulting in 100 snapshots. We computed VIEs for

each snapshot using EOM-IP-MP2/EFP and EOM-IP-MP2/MM. In the production runs, we used single-precision implementation of the CC/EOM-CC methods[15], which afforded speed-ups of more than 25%, while affecting the VIEs by less that 0.1 eV.

Our previous study[16] and benchmark calculations on the selected snapshots have shown that even with EFP, using the small QM subsystem with just arginine is not sufficient and that including explicit waters can change the VIEs considerably, i.e., by 0.2 eV for the lowest states and by more than 1 eV for the higher end of the band. Thus, in our calculations the QM region comprised the arginine and all water molecules that are hydrogen-bonded to it. Fig. S7 shows the distributions of the number of hydrogen bonds formed by different parts of arginine in different protonation states. As one can see, the number of hydrogen-bonded molecules varies between different forms of arginine. Depending on the conformer, the number of the explicit water molecules included in the QM region ranged from 5 to 10. We used a mixed basis set: aug-cc-pVDZ for heavy atoms and cc-pVDZ for hydrogens. The benchmark calculations for selected snapshots show that the VIEs computed with the truncated basis are within 0.1 eV from the full aug-cc-pVDZ calculation in the QM/MM simulations (Table S3). The resulting stick spectra were convoluted with 0.33 eV wide Gaussians, consistent with a typical resolution of synchrotron photon source.

**Benchmark calculations**. We used one snapshot of the *pg* structure to test and evaluate the effects of varying the level of theory. We considered EOM-IP-CCSD and EOM-IP-MP2 using EFP and TIP3P water model as the models. The QM region comprised the arginine together with all water molecules forming hydrogen bonds with it. The results are collected in Table S3.

Differences between the VIEs computed with different methods (EOM-IP-MP2 versus EOM-IP-CCSD) and basis sets do not exceed 0.2 eV. Therefore, in the production calculations of the photoionization spectra we employed EOM-IP-MP2 with the hybrid basis set, as the computational cost at this level of theory is significantly lower. The comparison between the QM/EFP and QM/MM results shows that the VIEs in the latter calculations appear to be systematically higher, ranging between 1.2 and 1.7 eV. This leads to a pronounced shift of the computed spectra, as shown in Fig. S8 for the *pg* form. Such large differences between non-polarizable and polarizable description of the solvent can be attributed to a strongly polar nature of arginine.
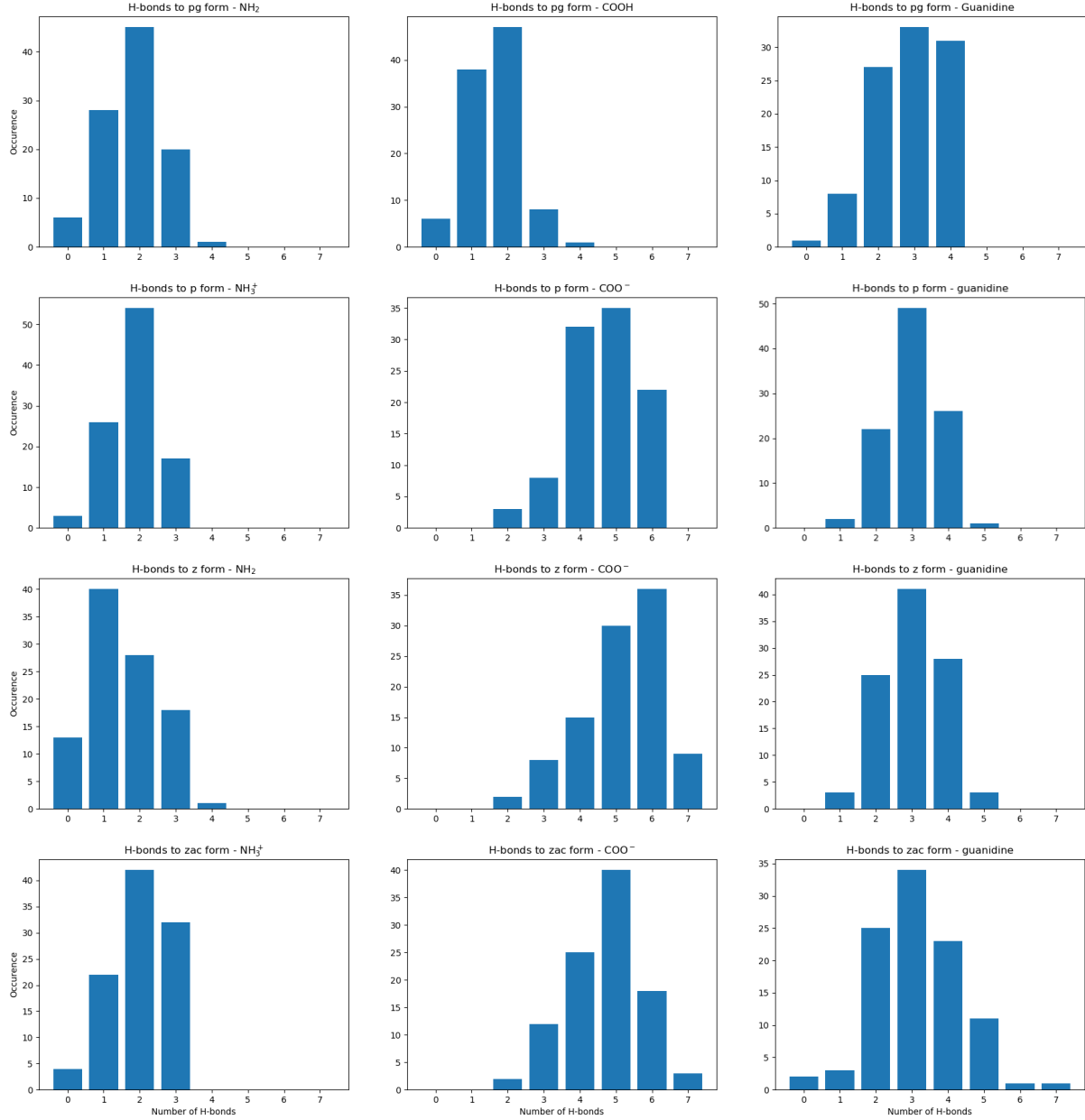
FIG. S7: Histograms showing the number of water molecules forming hydrogen bonds with different parts of arginine in the $p$, $pg$, $z$, and $zac$ forms. Statistics was obtained for 100 snapshots for each conformer.

## D.   Solvent effect in arginine spectra

As discussed in the section I E above, one needs to carefully account for the contribution of water photoionization in the computed spectra. On one hand, the inclusion of hydrogen-bonded water molecules in the QM subsystem is important for obtaining converged IEs, as illustrated by the previous studies[16] and our benchmark calculations. On the other hand, the

TABLE S3: VIEs for the 9 lowest EOM-IP states of arginine (*pg* form) in water for the first snapshot of the MD simulation. Energies were computed using EOM-IP-CCSD/EFP and EOM-IP-CCSD/MM with the mixed basis set (aug-cc-pVDZ for heavy atoms and cc-pVDZ for hydrogens) and the full aug-cc-pVDZ basis. This snapshot contains five water molecules hydrogen-bonded to arginine, which were included in the QM region. The last column shows the wall time of calculation in hours for each setup.

| Method | Vertical ionization energies (eV) | | | | | | | | | Time(h) |
|---|---|---|---|---|---|---|---|---|---|---|
| | EOM-IP-CCSD/EFP | | | | | | | | | |
| Mix-cc-pVDZ | 7.85 | 8.45 | 8.55 | 9.01 | 9.89 | 10.04 | 10.44 | 10.76 | 10.75 | 35 |
| aug-cc-pVDZ | 7.80 | 8.31 | 8.39 | 8.78 | 9.71 | 9.89 | 10.29 | 10.61 | 10.56 | 95 |
| | EOM-IP-MP2/EFP | | | | | | | | | |
| Mix-cc-pVDZ | 7.82 | 8.43 | 8.55 | 8.95 | 9.90 | 10.09 | 10.29 | 10.73 | 10.56 | 18 |
| aug-cc-pVDZ | 7.86 | 8.42 | 8.55 | 8.90 | 9.89 | 10.10 | 10.29 | 10.75 | 10.54 | 28 |
| | EOM-IP-CCSD/TIP3P | | | | | | | | | |
| Mix-cc-pVDZ | 9.25 | 9.64 | 10.07 | 10.28 | 11.23 | 11.31 | 11.88 | 12.04 | 12.20 | 24 |
| aug-cc-pVDZ | 9.27 | 9.66 | 10.08 | 10.29 | 11.24 | 11.32 | 11.89 | 12.05 | 12.21 | 62 |
| | EOM-IP-MP2/TIP3P | | | | | | | | | |
| Mix-cc-pVDZ | 9.26 | 9.61 | 10.07 | 10.21 | 11.21 | 11.28 | 11.76 | 11.93 | 12.11 | 6 |
| aug-cc-pVDZ | 9.28 | 9.62 | 10.08 | 10.21 | 11.22 | 11.30 | 11.77 | 11.95 | 12.12 | 20 |
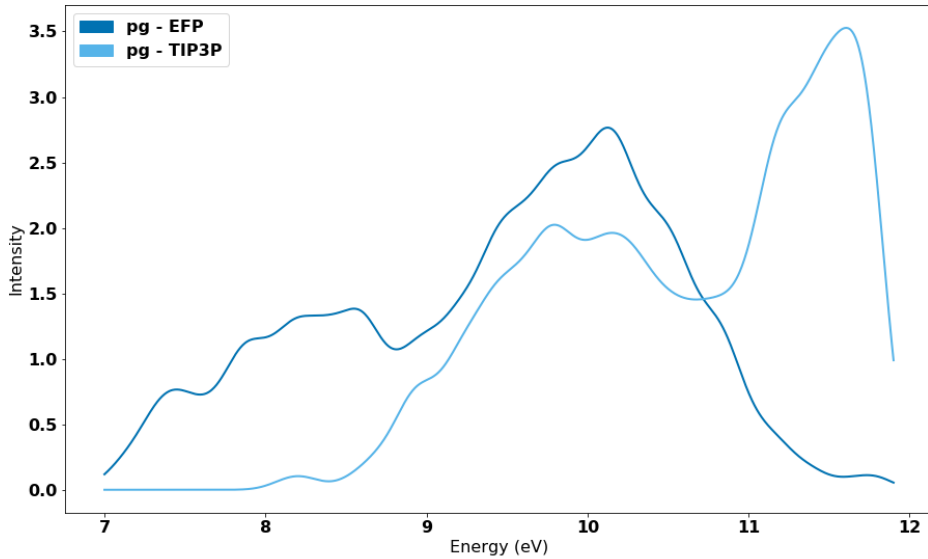


FIG. S8: Comparison of the computed photoelectron spectra of the *pg* form using the QM/MM and QM/EFP protocols.

QM water molecules can be ionized in the calculations, thus contributing to the computed

spectra. Consequently, EOM-IP calculations with large QM/MM can capture the states corresponding to ionization of water. Although representing the correct physical behavior, this complicates the interpretation and the assignment of the spectra.

The analysis of the Dyson orbitals shown in Figs. S9 and S10 illustrates the contributions of the explicit water molecules in the ionized states. As expected, the lowest ionized state (Fig. S9) is localized on arginine. However, higher-lying states, such as $9^{th}$ ionized state (shown in Fig. S10), feature significant contribution form water. This is not unexpected and fully consistent with the onset of bulk water ionization (Fig. S2). The IE of the waters that are hydrogen-bonded to arginine can drop even below the IE of bulk water. In particular, we anticipate significant effect for the water molecules hydrogen-bonded to the carboxylate group, where the negative charge on carboxylate stabilizes the ionized hole on the nearby water. On the basis of energy considerations, we expect that water contributions increase for higher states. While the appearance of water ionization is consistent with the electronic structure of water and arginine, it is not clear how to properly disentangle it from the arginine spectra. As discussed below, the contributions from water can vary for different forms (because of different hydrogen-bonding patters, Fig. S7), which can significantly distort the shape of the computed spectra. Unfortunately, we only computed Dyson orbitals for selected snapshots, which precludes us from quantitative characterization of the contribution from water for the entire dataset. Thus, we employed a somewhat empirical energy-based strategy, justified by the following observations.

To further analyze the extent of water contributions in the spectra, consider the stick spectra for six snapshots of the $p$ and $z$ conformers including VIEs below 10 eV shown in Fig. S11. The spectra shows two dense regions separated by a gap around 9 eV. The region between 9 and 10 eV is very dense and comprises most of the states. Note that in this region, the ionized states for the $p$ conformer tend to concentrate at higher energies than for $z$. This could be explained by the hydrogen-bond patterns between water and the carboxylate group for the two forms (Fig. S7): $z$-form has a higher number of bonds. Consequently, if one simply computes a histogram of all VIEs below 10 eV, the spectra of the $z$-form appears to be blue-shifted relative to the $p$-form, which contradicts basic electrostatic considerations (the protonated $p$-form is expected to have higher IEs) and experimental observation. To deal with this issue, we computed the spectra using several energy cutoffs: 9, 9.5 and 10 eV; the results are shown in Fig. S12. As one can see, the appearance of the spectra changes
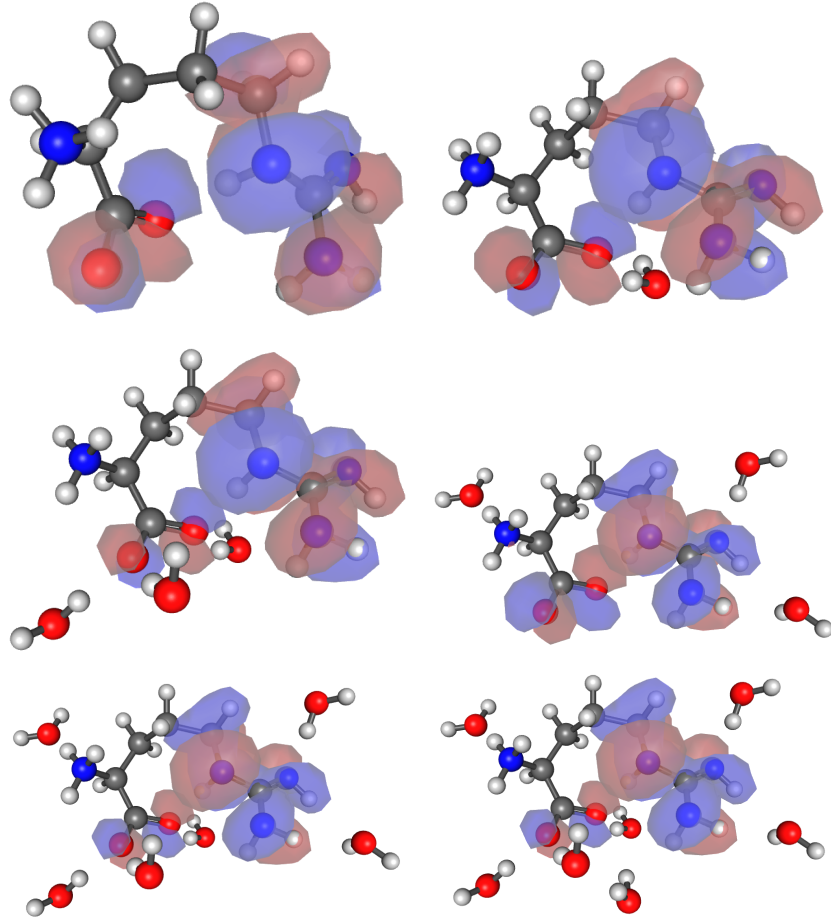
FIG. S9: Dyson orbitals corresponding to the first ionized state of arginine (*zac* form) computed by QM/MM with different number of water molecules in the QM region.

depending on the cutoff. The main effect is the increase of the lower band when using more aggressive cutoffs. Using a 9 eV cutoff causes a significant cut in the spectrum, whereas for 9.5 and 10 eV cutoff, most of the features of the spectra are preserved. Those two last cutoffs show the significant difference of a lower energy band maximum for the $z$-form, appearing to be red-shifted relative to the band maxima of the $p$-form. Particularly for 9.5 eV, the red shift is about 1 eV, consistent with the experimental trend.
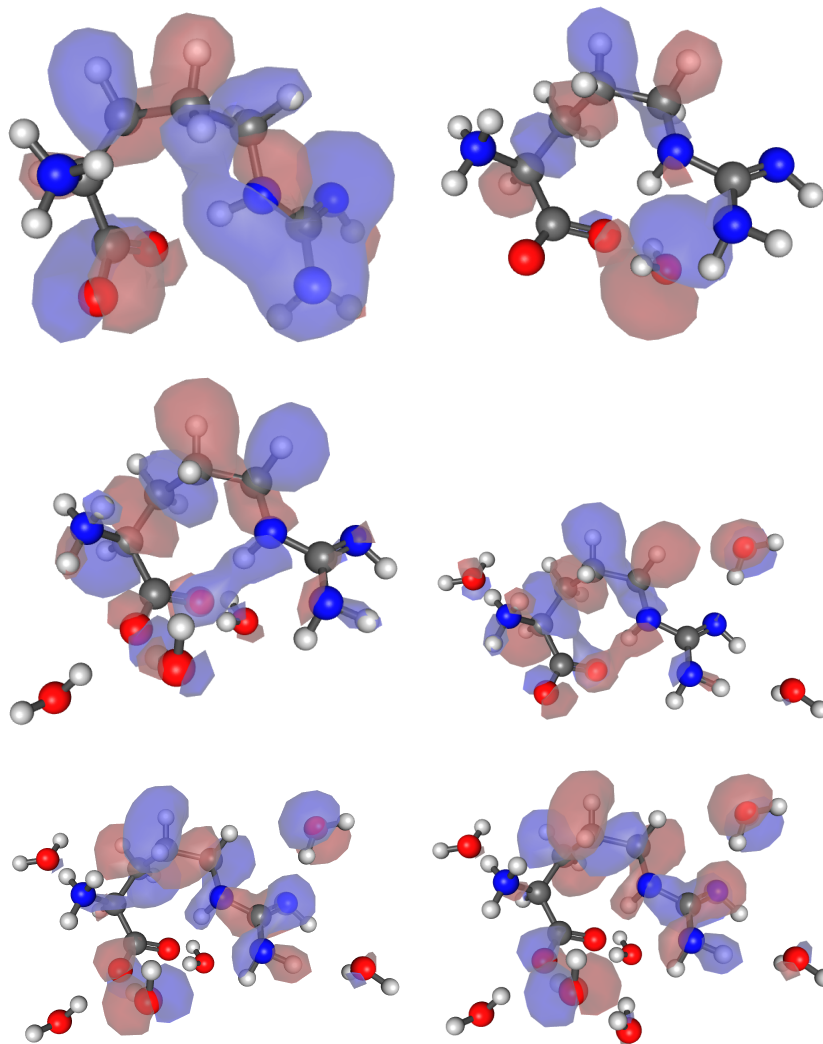
FIG. S10: Dyson orbitals corresponding to the 9th ionized state of arginine (*zac* form) computed by QM/MM with different number of water molecules in the QM region.
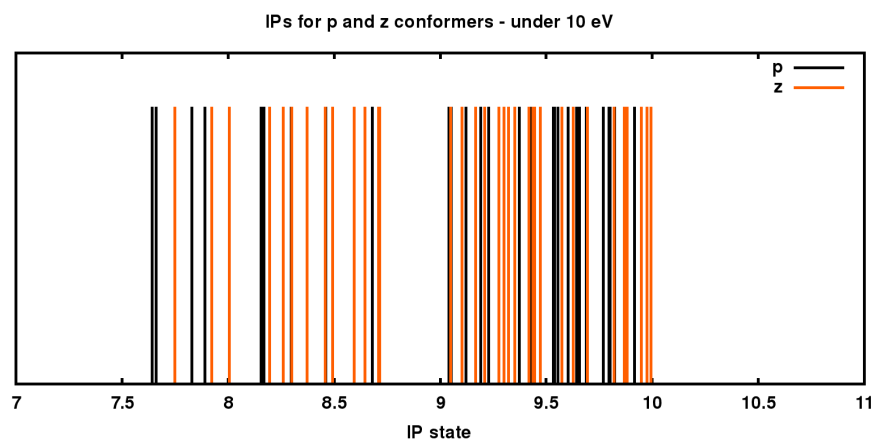


FIG. S11: Stick spectra for the *p* and *z* forms from the first six snapshots. Only IEs below 10 eV are shown.
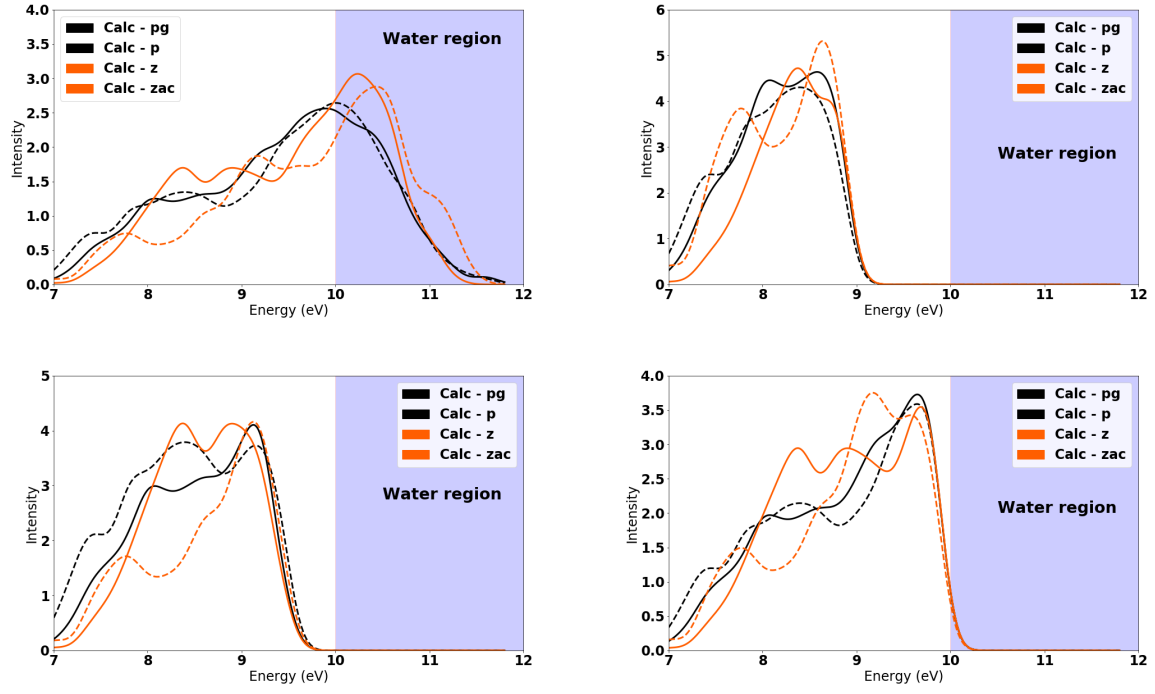
FIG. S12: Computed spectra for the *pg*, *p*, *z*, and *zac* forms with different energy cutoffs: no cutoff (top left), 9 eV (top right), 9.5 eV (bottom left), and 10 eV (bottom right), respectively.

[1] Wilson, K.R.; Belau, L.; Nicolas, C.; Jimenez-Cruz, M.; Leone, S.R.; Ahmed, M. Direct determination of the ionization energy of histidine with VUV synchrotron radiation *Int. J. Mass Spectrom.* **2006**, *249-250*, 155–161.

[2] Kostko, O.; Xu, B.; Jacobs, M. I.; Ahmed, M. Soft X-ray spectroscopy of nanoparticles by velocity map imaging *J. Chem. Phys.* **2017**, *147*, 013931.

[3] Parker, D.H.; Eppink, A. Velocity map imaging of ions and electrons using electrostatic lenses: Applications in photoelectron and photofragment ion imaging of molecular oxygen *Rev. Sci. Instr.* **1997**, *68*, 3477–3484.

[4] Dribinski, V.; Ossadtchi, A.; Mandelshtam, V.A.; Reisler, H. Reconstruction of Abel-transformable images: The Gaussian basis set expansion Abel transform method *Rev. Sci. Instrum.* **2002**, *73*, 2634–2642.

[5] Barth, S.; Ončák, M.; Ulrich, V.; Mucke, M.; Lischke, T.; Slavíček, P.; Hergenhahn, U. Valence ionization of water clusters: From isolated molecules to bulk *J. Phys. Chem. A* **2009**, *113*, 13519–13527.

[6] Winter, B.; Weber, R.; Widdra, W.; Dittmar, M.; Faubel, M.; Hertel, I.V. Full valence band photoemission from liquid water using EUV synchrotron radiation *J. Phys. Chem. A* **2004**, *108*, 2625–2632.

[7] Winter, B.; Faubel, M. Photoemission from liquid aqueous solutions *Chem. Rev.* **2006**, *106*, 1176.

[8] Webplotdigitizer. Rohatgi, A. https://automeris.io/WebPlotDigitizer; (Accessed January 2, 2019).

[9] Krylov, A. I.; Gill, P. M. W. Q-Chem: An engine for innovation *WIREs: Comput. Mol. Sci.* **2013**, *3*, 317–326.

[10] Shao, Y.; Gan, Z.; Epifanovsky, E.; Gilbert, A.T.B.; Wormit, M.; Kussmann, J.; Lange, A.W.; Behn, A.; Deng, J.; Feng, X., et al. Advances in molecular quantum chemistry contained in the Q-Chem 4 program package *Mol. Phys.* **2015**, *113*, 184–215.

[11] Hess, B.; Kutzner, C.; van der Spoel, D.; Lindahl, E. GROMACS 4: Algorithms for highly efficient, load-balanced, and scalable molecular simulation *J. Chem. Theory Comput.* **2008**, *4*, 435–447.

[12] Ling, S.; Yu, W.; Huang, Z.; Lin, Z.; Haranczyk, M.; Gutowski, M. Gaseous arginine conformers and their unique intramolecular interactions *J. Phys. Chem. A* **2006**, *110*, 12282–12291.

[13] Kaminski, G. A.; Friesner, R. A.; Tirado-Rives, J.; Jorgensen, W. L. Evaluation and reparametrization of the OPLS-AA force field for proteins via comparison with accurate quantum chemical calculations on peptides *J. Phys. Chem. B* **2001**, *105*, 6474–6487.

[14] Schlund, S.; Mueller, R.; Grassmann, C.; Engels, B. Conformational analysis of arginine in gas phase – a strategy for scanning the potential energy surface efficiently *J. Comput. Chem.* **2008**, *29*, 407–415.

[15] Pokhilko, P.; Epifanovskii, E.; Krylov, A. I. Double precision is not needed for many-body calculations: Emergent conventional wisdom *J. Chem. Theory Comput.* **2018**, *14*, 4088–4096.

[16] Sadybekov, A.; Krylov, A. I. Coupled-cluster based approach for core-ionized and core-excited states in condensed phase: Theory and application to different protonated forms of aqueous glycine *J. Chem. Phys.* **2017**, *147*, 014107.